The Astrophysical Journal Letters, 718:L97–L101, 2010 August 1 doi:10.1088/2041-8205/718/2/L97

EARLY ASTEROSEISMIC RESULTS FROM *KEPLER*: STRUCTURAL AND CORE PARAMETERS OF THE HOT B SUBDWARF KPD 1943+4058 AS INFERRED FROM *g*-MODE OSCILLATIONS

V. Van Grootel[1], S. Charpinet[1], G. Fontaine[2], P. Brassard[2], E. M. Green[3], S. K. Randall[4], R. Silvotti[5], R. H. Østensen[6], H. Kjeldsen[7], J. Christensen-Dalsgaard[7], W. J. Borucki[8], and D. Koch[8]

[1] Laboratoire d'Astrophysique de Toulouse-Tarbes, Université de Toulouse, CNRS, 14 av. E. Belin, 31400 Toulouse, France; valerie.vangrootel@ast.obs-mip.fr, stephane.charpinet@ast.obs-mip.fr

[2] Département de Physique, Université de Montréal, CP 6128, Succursale Centre-Ville, Montréal, QC H3C 3J7, Canada; fontaine@astro.umontreal.ca, brassard@astro.umontreal.ca

[3] Steward Observatory, University of Arizona, 933 North Cherry Avenue, Tucson, AZ 85721, USA; bgreen@as.arizona.edu

[4] ESO, Karl-Schwarzschild-Str. 2, 85748 Garching bei München, Germany; srandall@eso.org

[5] INAF-Osservatorio Astronomico di Torino, Strada dell'Osservatorio 20, 10025 Pino Torinese, Italy

[6] Instituut voor Sterrenkunde, K.U. Leuven, Celestijnenlaan 200D, 3001 Leuven, Belgium

[7] Department of Physics and Astronomy, Aarhus University, DK-8000 Aarhus C, Denmark

[8] NASA Ames Research Center, MS 244-30, Moffett Field, CA 94035, USA

Received 2010 June 4; accepted 2010 June 11; published 2010 July 8

ABSTRACT

We present a seismic analysis of the pulsating hot B subdwarf KPD 1943+4058 (KIC 005807616) on the basis of the long-period, gravity-mode pulsations recently uncovered by *Kepler*. This is the first time that *g*-mode seismology can be exploited quantitatively for stars on the extreme horizontal branch, all previous successful seismic analyses having been confined so far to short-period, *p*-mode pulsators. We demonstrate that current models of hot B subdwarfs can quite well explain the observed *g*-mode periods, while being consistent with independent constraints provided by spectroscopy. We identify the 18 pulsations retained in our analysis as low-degree ($\ell = 1$ and 2), intermediate-order ($k = -9$ through -58) *g*-modes. The periods (frequencies) are recovered, on average, at the 0.22% level, which is comparable to the best results obtained for *p*-mode pulsators. We infer the following structural and core parameters for KPD 1943+4058 (formal fitting uncertainties only): $T_{\rm eff} = 28{,}050 \pm 470$ K, $\log g = 5.52 \pm 0.03$, $M_* = 0.496 \pm 0.002\ M_\odot$, $\log (M_{\rm env}/M_*) = -2.55 \pm 0.07$, $\log (1 - M_{\rm core}/M_*) = -0.37 \pm 0.01$, and $X_{\rm core}({\rm C+O}) = 0.261 \pm 0.008$. We additionally derive the age of the star since the zero-age extended horizontal branch 18.4 ± 1.0 Myr, the radius $R = 0.203 \pm 0.007\ R_\odot$, the luminosity $L = 22.9 \pm 3.13\ L_\odot$, the absolute magnitude $M_V = 4.21 \pm 0.11$, the reddening index $E(B-V) = 0.094 \pm 0.017$, and the distance $d = 1180 \pm 95$ pc.

Key words: stars: individual (KPD 1943+4058) – stars: interiors – stars: oscillations – subdwarfs

Online-only material: color figure, machine-readable table

1. INTRODUCTION

KPD 1943+4058 is the brightest compact pulsator identified in the *Kepler* mission field (as KIC 005807616) and was the first to be spectroscopically confirmed as a subdwarf B (sdB) star. It is a relatively faint ($V = 14.87$) star originally found in the Kitt Peak-Downes survey of UV-excess objects in the galactic plane (Downes 1986). Except for the classification spectrum and *UBV* photometry provided by Downes, and the follow-up Strömgren (Wesemael et al. 1992) and *BVRI* (Allard et al. 1994) photometry, there is little else on KPD 1943+4058 in the literature. It was included by the Kepler Asteroseismic Science Consortium (KASC) as a potential seismic target for the survey phase at short cadence at 58.85 s (Gilliland et al. 2010), whose early results on compact stars are presented in Østensen et al. (2010). *Kepler* has revealed for KPD 1943+4058, through a spectacular light curve that will never be matched from the ground, some 26 distinct gravity-type pulsation modes, with periods ranging from about 2300 s up to 9200 s, and amplitudes larger than four times the local mean noise level. The list of periods extracted from the *Kepler* light curve is given in Table 1 (also see the consistent results of Reed et al. 2010).

Thanks to *Kepler*, we now have, for the first time, sufficiently high quality data for a detailed asteroseismological analysis of a long-period, *g*-mode variable. There have been successful seismic analyses of pulsating hot B subdwarfs (see, e.g., Van Grootel et al. 2008a, 2008b; Charpinet et al. 2008; Randall et al. 2009, and references therein), but those were all for short-period, *p*-mode pulsators. The *g*-modes offer probes of much deeper regions, because in hot B subdwarfs they propagate in the deep core while *p*-modes have non-negligible amplitudes in the outermost layers only (Charpinet et al. 2000).

Ever since their discovery at Steward Observatory (Green et al. 2003), it has been hoped that the long-period pulsating hot B subdwarfs would reveal the internal structure of the deepest regions in stars of this type, including their thermonuclear furnace. Despite valiant efforts from the ground (Randall et al. 2006a, 2006b), it has proved almost impossible to disentangle the true pulsation periods from the many aliases introduced by our inability to get continuous 24/7 observations, particularly in view of the very long periods and low amplitudes involved. With some prophetic flavor, Randall et al. (2006b, p. 1483) wrote in their conclusion: "Judging by our experience from the two ambitious multisite campaigns described in this short series of papers, the asteroseismic future of long-period variable sdB stars lies in space-based observations."

In this Letter, we exploit the exceptional data obtained on KPD 1943+4058 by *Kepler*. On this basis, we present a preliminary seismic analysis of a hot B subdwarf using *g*-mode pulsations. This is the first time that *g*-mode seismology can be performed for a core-helium burning star.

Table 1
List of Frequencies f_n (n is by Order of Decreasing Amplitude) Detected in KPD 1943+4058

ID		Period (s)	Frequency (μHz)	S/N	Comments
f_{15}	*	9126.39	109.572	5.6	
f_{19}	*	8371.11	119.459	4.6	
f_{21}	*	6677.44	149.758	4.5	
f_{13}	*	6199.51	161.303	9.6	
f_1	*	5959.80	167.791	88.5	
[f_4]		[5945.97]	[168.181]	[33.9]	[0.4 μHz from f_1]
f_7	*	5726.49	174.627	20.7	
f_2	*	5012.60	199.497	73.8	
f_9		4963.04	201.490	14.6	1.99 μHz from f_2
[f_{11}]		[4953.56]	[201.875]	[11.4]	[0.4 μHz from f_9]
[f_{23}]		[4941.73]	[202.358]	[4.8]	[0.4 μHz from f_{11}]
f_{22}	*	4427.21	225.876	5.4	
f_{10}	*	4272.51	234.055	13.1	
[f_{24}]		[4263.72]	[234.537]	[4.9]	[0.4 μHz from f_{10}]
f_8	*	4027.11	248.317	23.1	
[f_{18}]		[4007.73]	[249.518]	[6.9]	[0.4 μHz from f_{12}]
f_{12}		4001.33	249.917	11.5	1.62 μHz from f_8
f_6	*	3786.57	264.091	27.7	
[f_{14}]		[3784.15]	[264.261]	[9.0]	[<0.4 μHz from f_6]
f_{27}	*	3446.27	290.169	4.5	
f_5	*	3314.87	301.671	39.2	
f_{20}	*	3162.63	316.192	6.2	
f_{16}	*	2774.36	360.444	9.7	
f_{25}		2765.44	361.606	5.2	1.21 μHz from f_{16}
f_3	*	2540.58	393.611	52.7	
f_{17}	*	2475.51	403.957	9.3	
f_{26}	*	2346.37	426.190	5.7	
u_1		8929.10	111.993	3.3	
u_3		7054.19	141.760	3.2	
u_2		6923.24	144.441	3.6	
u_4		4698.13	212.851	3.8	
u_8		4530.72	220.715	3.7	
u_5		4138.26	241.648	3.8	
u_{10}		3859.92	259.073	3.7	
u_{11}		3731.33	268.001	3.5	
u_{13}		2899.48	344.889	3.6	
u_{14}		2043.50	489.357	3.7	
u_{12}		1969.62	507.712	3.8	
u_9		1492.96	669.812	4.0	
u_7		1214.50	823.387	4.0	
u_6		1212.22	824.935	4.0	

2. CONSTRAINTS FROM SPECTROSCOPY

Charpinet et al. (2005) have shown that the independent estimates for $T_{\rm eff}$ and log g provided by quantitative spectroscopy are essential input to avoid the degeneracies often encountered in seismic analyses of hot subdwarfs. In this respect, we were fortunate to have obtained a low-resolution (9 Å), moderately high S/N (∼112 in the blue) spectrum of KPD 1943+4058 with the Steward Observatory 2.3 m Bok Telescope. It was taken on 2008 12 June during a pre-launch search for hot subdwarfs in the *Kepler* field.

As part of the ongoing Tucson-Montréal spectroscopic program to characterize hot subdwarfs, we have now developed the capacity to compute non-LTE (NLTE) model atmospheres and synthetic spectra with arbitrary heavy-metal abundances and a large range of H and He compositions on a reasonable timescale. We used the most recent versions of the public codes TLUSTY and SYNSPEC made available and maintained by Ivan Hubeny (University of Arizona) and Thierry Lanz (University of Maryland) on their Web site (see, e.g., Hubeny & Lanz 1995; Lanz & Hubeny 1995, and Lanz et al. 1997 for details on some of the input physics). For the present application, we selected a representative heavy-element composition inspired from Blanchette et al. (2008). These authors used *FUSE* spectroscopy and suitable NLTE model atmospheres (again based on TLUSTY and SYNSPEC) to determine the abundances of several astrophysically important elements in the atmospheres of five typical long-period pulsating sdB stars similar to KPD 1943+4058. We recall here that hot subdwarfs are all chemically peculiar. The five stars analyzed by Blanchette et al. (2008) show very similar abundance patterns (see, e.g., their Figure 6), and we derived from these results a representative composition using the most abundant heavy elements. Hence, we assumed atmospheres containing C (1/10 solar), N (solar), O (1/10 solar), Si (1/10 solar), S (solar), and Fe (solar).

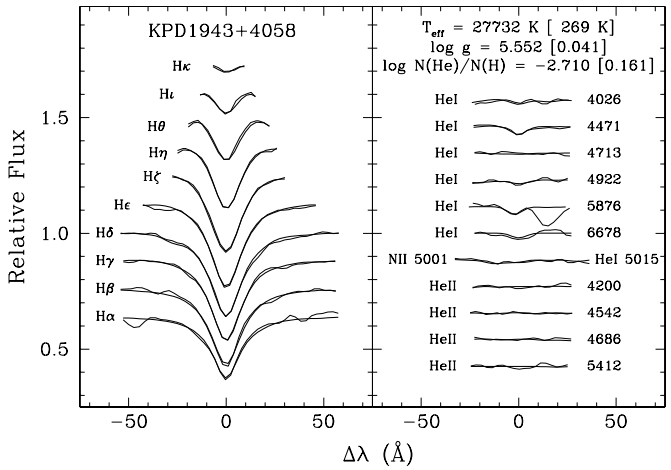

Figure 1. Model fit (heavy curve) to all the hydrogen and strong helium lines (thin curve) available in our moderately high S/N, low-resolution optical spectrum of KPD 1943+4058. The fit was done using a three-dimensional grid of NLTE synthetic spectra ($T_{\rm eff}$, log g, log N(He)/N(H)) in which the abundances of C, N, O, S, Si, and Fe were held fixed at amounts consistent with Blanchette et al. (2008). The only detectable metal line is the N II 5001 feature. It is the strongest of all predicted metal lines in our fitted theoretical spectrum, the other weaker features having all but been wiped out by the limited resolution. Some signs of interstellar absorption are revealed by the presence of the well-known Na I doublet in the red wing of the He I 5876 line and of a weak Ca II K feature in the blue wing of Hϵ.

Figure 1 shows the result for our best fit. We find $T_{\rm eff}$ = 27,730 ± 270 K, log g = 5.552 ± 0.041, and log N(He)/N(H) = −2.71 ± 0.16. The quoted uncertainties are only formal errors of the fit and do not include external errors, which remain difficult to evaluate in the absence of multiple observations. The overall fit to the full spectrum is quite good, but we note that the signal-to-noise ratio (S/N) deteriorates significantly in the redder part, thus driving the formal uncertainties to relatively large values. We also note that the strongest predicted metal line (an N II complex around 5001 Å) is just barely detected at about the correct strength (for a solar abundance of N), while all the other numerous but weaker predicted metal features are not. This is simply a consequence of the limited resolution (9 Å) at work here which practically washes away all these features, even in our noiseless model spectrum. Thus, even though our detection of N at roughly solar abundance is encouraging, we cannot be entirely certain at this stage that the atmosphere of KPD 1943+4058 contains all the elements identified in the Blanchette et al. (2008) study. To provide a measure of the uncertainties associated with the presence (or the absence) of metals, we have refitted our spectrum with NLTE atmosphere models

containing only H and He. We now find $T_{\rm eff} = 28{,}180 \pm 280$ K, $\log g = 5.549 \pm 0.042$, and $\log N({\rm He})/N({\rm H}) = -2.71 \pm 0.16$, thus indicating that the presence of metals is not a critical issue in the determination of the atmospheric parameters of KPD 1943+4058.

3. DETAILED ASTEROSEISMIC ANALYSIS

3.1. Models and Method

For the seismic analysis we used the same forward-modeling approach successfully employed in the study of *p*-mode sdB pulsators. The method has been described in detail in Charpinet et al. (2005, 2008). The basic principle is to simultaneously fit all of the observed pulsation periods with theoretical ones calculated for appropriate stellar models, in order to minimize in parameter space a merit function defined by

$$S^2 = \sum_{i=1}^{N_{\rm obs}} \left(P^i_{\rm obs} - P^i_{\rm th}\right)^2, \qquad (1)$$

where $N_{\rm obs}$ is the number of observed periods and $\{P^i_{\rm obs}, P^i_{\rm th}\}$ are the associated pairs of observed/computed periods. Efficient optimization codes have been developed to explore the vast model parameter space and find the minima of the merit function S^2, which constitute the potential asteroseismic solutions. The results of this procedure are the mode identification and, more importantly, the structural parameters of the star.

In order to carry out quantitative seismology of *g*-mode pulsators, we had to improve upon the models that we used for short-period variables. We thus developed our "third-generation" (3G) models, now suitable for the accurate evaluation of *g*-mode pulsation periods. Details about our 3G models are given in Brassard & Fontaine (2008, 2009). In a nutshell, these are complete stellar structures in thermal equilibrium and are defined in terms of a set of parameters inspired from full evolutionary models. The reason we prefer to use such static parameterized structures over evolutionary models is that the former provide a much needed flexibility for thoroughly exploring parameter space.

The input parameters needed to characterize a 3G model are (1) the total stellar mass M_*, (2) the fractional mass of the outer hydrogen-rich envelope $\log (M_{\rm env}/M_*)$, (3) the fractional mass of the mixed convective core $\log (M_{\rm core}/M_*)$, and (4) the chemical composition of the core (under the constraint $X({\rm He})+X({\rm C})+X({\rm O})=1$). The effective temperature $T_{\rm eff}$ and surface gravity $\log g$ are computed a posteriori for a given 3G model. We therefore now incorporate the atmospheric parameters determined by spectroscopy as external constraints in the optimization procedure for the search of a best-fit model. Only those models defined by minima in the S^2 merit function that have atmospheric parameter values within 3σ of the spectroscopic estimates are considered acceptable, thus ensuring, by construction, consistency with spectroscopy. In the specific case of KPD 1943+4058, acceptable solutions have to fall in the ranges of parameters defined by $T_{\rm eff} = 27{,}730 \pm 810$ K and $\log g = 5.552 \pm 0.123$. Note that there is no guarantee, a priori, that a good period match exists within these constraints.

3.2. Search for the Optimal Model

The present asteroseismic analysis is based on a subset of the frequencies given in Table 1. Among these, several frequencies (f_4, f_{11}, f_{23}, f_{24}, f_{18}, and f_{14}) are in fact very close to peaks of higher amplitude in the pulsation spectrum (f_1, f_9, f_{11}, f_{10}, f_{13}, f_6, respectively). The separation is $\sim$0.4 μHz, which is of the order of the data frequency resolution. These components are therefore not well resolved with the present data set. It is not clear, at this stage, if they are associated with components of multiplets split by slow rotation (as the usual case of single sdB stars) or with residual structure from the prewhitening of a dominant frequency whose amplitude and/or phase experienced significant changes during the run. This issue is not critical for our present analysis and we decided to ignore them, which left us with 21 pulsation modes. The frequency spectrum also presents three pulsations showing a frequency spacing close to a multiple of 0.4 μHz (f_9 is 1.99 μHz away from f_2, f_{12} is 1.62 μHz away from f_8, and f_{25} is 1.21 μHz away from f_{16}). If rotation is involved, these could be components of multiplets, so they too were excluded from the first step of the analysis. This restricts the asteroseismic procedure to 18 pulsation periods that can be safely assumed to be independent. We stress that the remaining 18 periods (identified by asterisks in Table 1) provide enough modes to tightly constrain the asteroseismic solution. The additional suspected pulsation modes u_1 to u_{14} (with amplitudes between 3.2 and 4 times the local noise level) were also neglected in the asteroseismic analysis that follows. This conservative approach limits the risk of biasing the model search by using signals that may turn out to be spurious. Nonetheless, we will discuss a posteriori how these additional frequencies may be interpreted and compared to the theoretical periods of the optimal model solution uncovered.

The search for best-fit solutions was carried out in the following domain: $0.30 \leqslant M_*/M_\odot \leqslant 0.70$, $-5.0 \leqslant \log q({\rm H}) \equiv \log(M_{\rm env}/M_*) \leqslant -1.8$, $-0.40 \leqslant \log q({\rm core}) \equiv \log(1 - M_{\rm core}/M_*) \leqslant -0.10$, and $0 \leqslant X_{\rm core}({\rm C+O}) \leqslant 0.99$, where $X_{\rm core}$(C+O) is the fractional part (in mass) of carbon and oxygen in the convective core.[9] The ranges considered for $\log q$(H) and M_* rely on predictions from various formation scenarios for hot subdwarfs (Han et al. 2002, 2003), whereas the limits on the core size are loosely inspired by horizontal branch stellar evolutionary calculations (Dorman et al. 1993). We considered all modes of degrees $\ell = 1$ and 2 in the 2000–9500 s period range in order to match the 18 pulsation periods. The upper limit of the degree ℓ corresponds to the minimum value that accounts for the observed mode density. No other assumption on the mode identification has been imposed.

Within the search domain specified, and taking into consideration the external constraints on atmospheric parameters, the optimization code isolated a clear deep minimum that constitutes the seismic solution. The parameters of this model solution are $M_* = 0.4964\ M_\odot$, $\log q({\rm H}) = -2.553$, $\log q({\rm core}) = -0.366$, and $X_{\rm core}({\rm C+O}) = 0.2612$, leading to $T_{\rm eff} = 28{,}050$ K and $\log g = 5.5204$. This is in excellent agreement with spectroscopic estimates, within 1.2σ and 0.8σ uncertainties for the effective temperature and surface gravity, respectively. The maps shown in Figure 2 illustrate the behavior of the merit function in the vicinity of the best-fit seismic solution.

In both panels, the merit function S^2 incorporates the spectroscopic constraints on atmospheric parameters. To create these plots, we tolerated a deviation of 2σ for the effective temperature and 1σ for the surface gravity, i.e., S^2 is uncorrected if the models have $T_{\rm eff} = 27{,}730 \pm 540$ K and $\log g = 5.552 \pm 0.041$. An exponential correction factor multiplies the merit function if the model effective temperature and surface

[9] We have found that theoretical periods are not very sensitive to the exact core composition of C and O. Grouping (C+O) in one parameter facilitates and speeds up the optimization procedure.

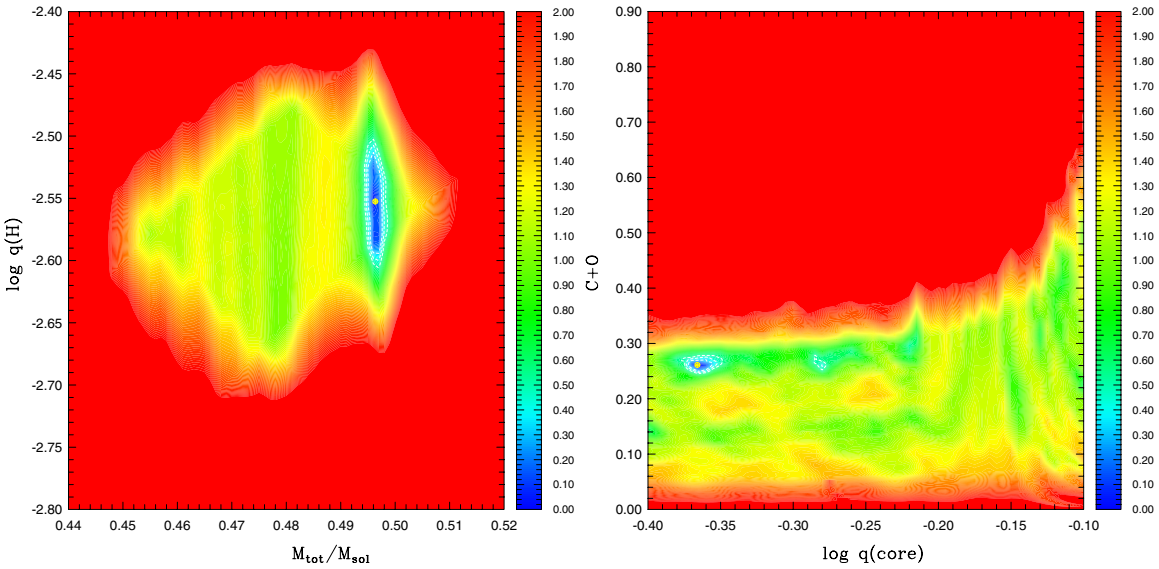

Figure 2. Left panel: slice of the S^2 function (in logarithmic units) along the $M_* - \log q(\mathrm{H})$ plane with the parameters $\log q(\mathrm{core})$ and $X_{\mathrm{core}}(\mathrm{C+O})$ fixed to their optimal values obtained in the best-fit seismic model. Right panel: slice of the S^2 function (in log) along the $\log q(\mathrm{core}) - X_{\mathrm{core}}(\mathrm{C+O})$ plane with the parameters M_* and $\log q(\mathrm{H})$ fixed to their optimal values. White contours show regions where the period fits have S^2 values within, respectively, the 1σ, 2σ, and 3σ confidence levels relative to the best-fit solution.

(A color version of this figure is available in the online journal.)

Table 2
Mode Identification and Other Properties

ℓ	k	ν_{obs} (μHz)	ν_{th} (μHz)	P_{obs} (s)	P_{th} (s)	$\log E$ (erg)	C_{kl}	$\Delta X/X$ (%)	ΔP (s)	$\Delta\nu$ (μHz)	ID
1	−3	···	1071.115	···	933.61	45.985	0.5956	···	···	···	
1	−4	[824.935]	826.453	[1212.22]	1209.99	47.384	0.4579	[+0.18]	[+2.23]	[−1.518]	[u_6]
1	−5	···	661.624	···	1511.43	47.791	0.4550	···	···	···	
1	−8	···	454.406	···	2200.68	45.448	0.4829	···	···	···	
1	−9	393.611	392.554	2540.58	2547.42	46.382	0.4886	−0.27	−6.84	+1.056	f_3

(This table is available in its entirety in a machine-readable form in the online journal. A portion is shown here for guidance regarding its form and content.)

gravity are outside these ranges, in effect degrading the S^2 value of the model. The panels clearly indicate deep blue regions (corresponding to best-fitting models, i.e., low values of S^2) in the $M_* - \log q(\mathrm{H})$ and $\log q(\mathrm{core}) - X_{\mathrm{core}}(\mathrm{C+O})$ planes, well defined by the pulsation spectrum and the spectroscopic constraints. The regions in red correspond to models that are not consistent with spectroscopic values within the 2σ and 1σ tolerance mentioned above.

3.3. Period Fit and Mode Identification

The optimal model isolated for KPD 1943+4058 presents an excellent simultaneous match to the 18 observed periods retained for asteroseismology. Details on the fit and the mode identification are given in Table 2. The averaged relative dispersion is $\overline{\Delta X/X} \sim 0.22\%$ (where $X = P$ or ν), which corresponds, on an absolute scale, to $\overline{\Delta P} = 7.80$ s and $\overline{\Delta\nu} = 0.697$ μHz. The standard deviations on these quantities are, respectively, 4.64 s and 0.924 μHz. The quality of the fit is comparable to the best results obtained for p-mode pulsators, which typically rely on fewer observed periods and include $\ell = 0, 1, 2$, and 4 pulsation modes. The 18 pulsations retained in our analysis are identified as low-degree ($\ell = 1$ and 2), intermediate-order ($k = -9$ through -58) g-modes.

It is interesting to look back at Table 1 and see how the additional frequencies may be interpreted in the theoretical spectrum of the identified optimal model. Among the frequencies left aside, f_9 (201.490 μHz) and f_{12} (249.917 μHz) find correspondences with $\ell = 2, k = -34$ (199.946 μHz) and $\ell = 1, k = -15$ (249.161 μHz), respectively. These two matches do not degrade the overall fit. f_{25} (361.606 μHz) has no equivalent in the $\ell = 1$ and $\ell = 2$ series. This can be solved, however, if the moderately dense $\ell = 4$ spectrum (which are the most visible modes after $\ell = 1$ and $\ell = 2$ in sdB stars; Randall et al. 2005) is invoked. Indeed, in this model an $\ell = 4, k = -34$ mode at 363.651 μHz matches f_{25} at an acceptable accuracy. This mode, found at just ∼5.2 times the noise level, has a very low amplitude and its identification with an $\ell = 4$ mode is reasonable. Thirteen out of the fourteen additional frequencies u_n find a corresponding mode in the $\ell = 1$ and $\ell = 2$ series without significantly degrading the fit (see details in Table 2). The remaining additional frequency u_{12} (at 507.712 μHz) finds a correspondence if, again, $\ell = 4$ modes are allowed (506.229 μHz for the mode $\ell = 4, k = -24$). In summary, all the observed pulsation spectrum can be explained by modes of degrees $\ell = 1$ and 2, with only two exceptions for two very low amplitude pulsation modes which can be accommodated if $\ell = 4$ is allowed.

Table 3
Structural and Core Parameters Inferred for KPD 1943+4058 (All the Quoted Uncertainties are the Formal Fitting Ones)

Quantity	Estimated Value
$T_{\rm eff}$ (K)	27730 ± 270[a]
	28050 ± 470[b]
$\log g$	5.552 ± 0.041[a]
	5.52 ± 0.03[b]
$M_*/M_\odot$	0.496 ± 0.002
$\log(M_{\rm env}/M_*)$	−2.55 ± 0.07
$\log(1 - M_{\rm cc}/M_*)$	−0.37 ± 0.01
$M_{\rm cc}/M_\odot$	0.28 ± 0.01
$X_{\rm core}$(C+O)	0.261 ± 0.008
Age (Myr)	18.4 ± 1.0[c]
$R/R_\odot$ (M_*, g)	0.203 ± 0.007
$L/L_\odot$ ($T_{\rm eff}$, R)	22.9 ± 3.1
M_V (g, $T_{\rm eff}$, M_*)	4.21 ± 0.11
$E(B-V)$	0.094 ± 0.017
d (V, M_V) (pc)	1180 ± 95

Notes.
[a] From spectroscopy.
[b] From asteroseismology.
[c] Since zero-age EHB.

3.4. Structural and Core Parameters

The asteroseismic analysis leads to the determination of the basic structural parameters of KPD 1943+4058, as summarized in Table 3. Estimates of the 1σ (internal) uncertainties associated with the primary quantities (those naturally derived from the asteroseismic analysis) are calculated following the recipe described in detail in Brassard et al. (2001) and Charpinet et al. (2005). These uncertainties are represented in Figure 2 by white dashed contours (1σ, 2σ, and 3σ limits) around the solution indicated by a yellow mark. The uncertainties on the derived atmospheric parameters $T_{\rm eff}$ and $\log g$ are obtained from the uncertainties of the primary quantities. A set of secondary parameters (stellar radius R, luminosity L, absolute magnitude M_V, reddening index $E(B-V)$, and distance from Earth d) is also derived on the basis of primary parameters. All the uncertainties quoted in Table 3 are statistical ones, with the understanding that the true uncertainties due to systematic effects are probably larger, but difficult to estimate.

The total mass of KPD 1943+4958 inferred is close to the canonical value expected for hot B subdwarfs (Dorman et al. 1993; Han et al. 2002, 2003). The hydrogen-rich envelope is thicker than envelopes measured so far in short-period pulsating sdB stars. This conforms to the expected correlation between $T_{\rm eff}$ and $M_{\rm env}$ (cooler extreme horizontal branch stars should have thicker envelopes). Of utmost interest are the parameters related to the helium-burning core. It was hoped that g-modes in sdB stars could probe the properties of the core, and they do. The mixed convective core is found to be rather massive, including more than half (57%) of the total mass of the star, while it has burned only a little over 25% of its helium nuclear fuel. This size is significantly above what is expected from evolutionary tracks computed by Dorman et al. (1993). These authors, however, defined the convective core by the Schwarzschild criterion and did not consider overshooting, while the chemical transition He/C/O–He defines its boundary in our models. Our measurement may therefore be the signature of an extended core due to overshooting, i.e., the fact that processed material (C+O) is carried out by momentum beyond the convection zone itself. A comparison with an evolutionary sequence built on the same input physics for a star with similar structural and core parameters indicates an age of 18.4 ± 1.0 Myr after the zero-age extended horizontal branch (EHB).

4. CONCLUSION

In this Letter, we have presented the first asteroseismic analysis of a hot subdwarf based on g-mode pulsations, thanks to the outstanding photometric data obtained from space by *Kepler* on KPD 1943+4058. The optimal model uncovered offers an excellent fit, with a relative dispersion of ∼0.22%, to 18 observed periods that are identified with theoretical modes of degrees $\ell = 1$ and 2. The inferred structural parameters for KPD 1943+4058 include the total stellar mass, the thickness of the hydrogen-rich envelope, and the size and the composition of the convective core. Some of these quantities cannot be derived using other means and are invaluable for understanding sdB stars' evolutionary history.

This is the first time that g-mode seismology has been used to investigate core-helium burning/horizontal branch stars. Our results suggest that overshooting is an important process shaping the helium burning core. Since all helium-burning cores share very similar characteristics, pulsating B subdwarfs are excellent probes of the interior properties of horizontal branch stars in general, an intermediate stage of stellar evolution experienced by the vast majority of stars during their lifetime.

Funding for the *Kepler* Mission is provided by NASA's Science Mission Directorate. We gratefully acknowledge the Kepler Science Team and all those who have contributed to making the *Kepler* Mission possible. We thank WG11 members for helpful discussions. V.V.G. acknowledges grant support from the Centre National d'Etudes Spatiales (CNES).

REFERENCES

Allard, F., Wesemael, F., Fontaine, G., Bergeron, P., & Lamontagne, R. 1994, AJ, 107, 1565
Blanchette, J.-P., et al. 2008, ApJ, 678, 1329
Brassard, P., et al. 2001, ApJ, 563, 1013
Brassard, P., & Fontaine, G. 2008, in ASP Conf. Ser. 392, Hot Subdwarf Stars and Related Objects, ed. U. Heber, C. S. Jeffery, & R. Napiwotzki (San Francisco, CA: ASP), 261
Brassard, P., & Fontaine, G. 2009, J. Phys. Conf. Ser., 172, 2016
Charpinet, S., Fontaine, G., Brassard, P., & Dorman, B. 2000, ApJS, 131, 223
Charpinet, S., et al. 2005, A&A, 437, 575
Charpinet, S., et al. 2008, A&A, 489, 377
Dorman, B., Rood, R. T., & O'Connell, R. W. 1993, ApJ, 419, 596
Downes, R. A. 1986, ApJS, 61, 569
Gilliland, R. L., et al. 2010, ApJ, 713, L160
Green, E. M., et al. 2003, ApJ, 583, L31
Han, Z., Podsiadlowski, P., Maxted, P., & Marsh, T. R. 2003, MNRAS, 341, 669
Han, Z., Podsiadlowski, P., Maxted, P., Marsh, T. R., & Ivanova, N. 2002, MNRAS, 336, 449
Hubeny, I., & Lanz, T. 1995, ApJ, 439, 875
Lanz, T., & Hubeny, I. 1995, ApJ, 439, 905
Lanz, T., Hubeny, I., & Heap, S. R. 1997, ApJ, 485, 843
Østensen, R. H., et al. 2010, MNRAS, submitted
Randall, S. K., Fontaine, G., Brassard, P., & Bergeron, P. 2005, ApJS, 161, 456
Randall, S. K., et al. 2006a, ApJ, 643, 1198
Randall, S. K., et al. 2006b, ApJ, 645, 1464
Randall, S. K., et al. 2009, A&A, 507, 911
Reed, M. D., et al. 2010, MNRAS, submitted
Van Grootel, V., Charpinet, S., Fontaine, G., & Brassard, P. 2008a, A&A, 483, 875
Van Grootel, V., et al. 2008b, A&A, 488, 685
Wesemael, F., Fontaine, G., Bergeron, P., Lamontagne, R., & Green, R. 1992, AJ, 104, 203